ISSN 0965-5425, Computational Mathematics and Mathematical Physics, 2024, Vol. 64, No. 10, pp. 2388–2398. © Pleiades Publishing, Ltd., 2024.

MATHEMATICAL PHYSICS

Verification of a Numerical Algorithm Based on Quasi-Hydrodynamic Equations as Applied to Thermal Convection Problems

M. A. Kiryushina[a,*], T. G. Elizarova[a], and A. S. Epikhin[b]

[a] *Federal Research Center Keldysh Institute of Applied Mathematics, Russian Academy of Sciences, Moscow, 125047 Russia*

[b] *Ivannikov Institute for System Programming of the Russian Academy of Sciences, Moscow, 109004 Russia*

**e-mail: m_ist@mail.ru*

Received November 23, 2023; revised April 18, 2024; accepted June 28, 2024

Abstract—It is shown that the quasi-hydrodynamic (QHD) algorithm allows one to simulate viscous uncompressible flows in thermal convection problems at large Grashof numbers, including the correct description of the onset of an oscillatory process. Tests for square and rectangular cavities are described. The computations are performed by applying the QHD algorithm incorporated into the OpenFOAM package.

Keywords: control volume method, OpenFOAM package, quasi-hydrodynamic algorithm, viscous incompressible fluid, thermal convection

DOI: 10.1134/S0965542524701331

INTRODUCTION

The evaluation of the capabilities of algorithms for modeling thermal convection is required for the subsequent adequate choice of a numerical algorithm. Of particular interest are flows with unsteady regimes that may precede the onset of a laminar–turbulent transition. Theoretical studies of the stability threshold and parameters of secondary convective flows in thermal convection problems can be found, for example, in the classical monograph [1]. Experimental studies of flow stability have been conducted in a wide range of Grashof (Gr) and Prandtl (Pr) numbers. Specifically, the instability of thermal convection at large Pr values of order 20 was observed in experiments with ethyl alcohol [2], while unstable flows at small Pr values of order 0.01 arose in melt flow problems [3].

For thermal convection problems in the Boussinesq approximation, flows in square and rectangular cavities in two-dimensional setting for Pr numbers of order 1 serve as indicative and convenient numerical benchmark tests for determining the onset of oscillations. These benchmark problems are used because of the simplicity of their formulations and the simultaneous complexity of developing flows. Numerous results obtained for them allow one to perform an objective evaluation of tested methods. Of particular interest in these problems is the transition from steady-state flow to unsteady one, which occurs with an increase in the Grashof or Rayleigh number. A detailed overview of results of modeling thermal convection in rectangular cavities produced by various algorithms is hardly possible. We note only several recent works [4–9] (see also the bibliography therein). They involve high-order methods in time and space applied to equations written in terms of stream function–vorticity and velocity–pressure variables [4, 5], Lattice Boltzmann algorithms for a compressible gas at low Mach numbers [6, 9], spectral methods [7], and methods with locally refined spatial grids [8]. These benchmark tests were also used to verify individual aspects of open-source software for fluid dynamics problems, a survey of which can be found in [10].

In this paper, thermal convection in square and rectangular cavities is modeled to test the performance of a numerical algorithm based on regularized, or quasi-hydrodynamic (QHD) equations governing viscous incompressible fluid flows. A description of the QHD equations can be found, for example, in [11–13]. A number of results on testing the numerical algorithm for the above problems within the framework of research programs are given in [11–14], where two-dimensional flows were considered in flat and cylindrical geometry with an approximation based on rectangular grids without parallelization of computations. Later, an improved version of the algorithm was developed, which involved three-dimensional

unstructured meshes and an opportunity for parallelization. This version of the algorithm was incorporated as a separate module in the open-source OpenFOAM package [15], which is able to deal with computational domains of complex geometry and to use multiprocessor computing systems to speed up computations. A new version of the QHD algorithm as applied to the computation of thermal convection was described in [16]. Below, its further modified version is tested on well-known two-dimensional thermal convection problems, including the transition to an unsteady flow regime at high Grashof numbers.

The QHD equations for thermal convection problems in the Boussinesq approximation are described in Section 1. Additionally, a brief description of the numerical algorithm is presented. In Section 2, we consider thermal convection in a square cavity at high Grashof numbers. The transition from steady flow to unsteady one is traced. The results allow us to refine the settings of the algorithm, estimate the convergence of the numerical solution on a sequence of refined grids, and compare the numerical results with data available in the literature. The unsteady convection problem in a 1:8 rectangular cavity at the Rayleigh number $\mathrm{Ra} = 3.4 \times 10^5$ is considered in Section 3. The resulting conclusions are given in Section 4.

1. QHD EQUATIONS AND NUMERICAL ALGORITHM

For numerical modeling, we use the QHD method based on a regularization of the Navier–Stokes equations. The equations are regularized assuming that the mass density of the fluid flow differs from the average momentum of a unit volume by a small value. This difference leads to small dissipative additives appearing in the original equations. These terms have a physical nature and allow using a conditionally stable explicit difference scheme with all spatial derivatives approximated by central differences.

Following [11–14], the QHD system of equations in the Oberbeck–Boussinesq approximation is written as

$$\operatorname{div}(\mathbf{u} - \mathbf{w}) = 0, \tag{1}$$

$$\frac{\partial \mathbf{u}}{\partial t} + \operatorname{div}((\mathbf{u} - \mathbf{w}) \otimes \mathbf{u}) + \frac{1}{\rho_0}\nabla p = \frac{1}{\rho_0}\operatorname{div}\Pi - \beta \mathbf{g}(T - T_0), \tag{2}$$

$$\frac{\partial T}{\partial t} + \operatorname{div}((\mathbf{u} - \mathbf{w})T) = x\Delta T. \tag{3}$$

The velocity correction vector $\mathbf{w}$ and the viscous stress tensor Π are given by

$$\mathbf{w} = \tau\left[(\mathbf{u}\cdot\nabla)\mathbf{u} + \frac{1}{\rho_0}\nabla p + \beta \mathbf{g}(T - T_0)\right], \quad \Pi = \Pi_{NS} + \rho_0 \mathbf{u} \otimes \mathbf{w}. \tag{4}$$

Here, τ is the regularization parameter, which has the dimension of time. The QHD system is closely related to the original Navier–Stokes system, and they have a number of common exact solutions. In particular, for the steady flow between two differently heated vertical infinite plates under gravity, the Navier–Stokes exact solution given in [1] is also the exact solution of this problem for the QHD equations [11]. For $\tau = 0$, the regularized system turns into the original system of equations.

Numerical simulations of viscous incompressible flows have shown that spurious oscillations may appear in the numerical solution of the temperature equation (3) when the velocity of forced convection is high, while the thermal conductivity is low. This suggests that the regularizer introduced into the equation (which is determined by the quantity $\mathbf{w}$ in (4)) is insufficient. These numerical oscillations are smoothed out by introducing another smoothing term into the right-hand side of Eq. (3), which then becomes

$$\frac{\partial T}{\partial t} + \operatorname{div}(\mathbf{u}T) = \operatorname{div}(\mathbf{w}T) + \chi\Delta T + \operatorname{div}(\tau\mathbf{u}(\mathbf{u}\cdot\nabla T)). \tag{5}$$

This type of regularization for the temperature equation is used in the algorithm implemented in the OpenFOAM package [15, 16].

In contrast to the Navier–Stokes equations, the Poisson equation for pressure in the QHD system follows directly from the continuity equation. Indeed, substituting the expression for $\mathbf{w}$ given by (4) into the continuity equation (1), we immediately obtain the following pressure equation at constants ρ_0 and τ:

$$\frac{1}{\rho_0}\Delta p = -\operatorname{div}[(\mathbf{u}\cdot\nabla)\mathbf{u}] + \frac{1}{\tau}\operatorname{div}\mathbf{u} - \operatorname{div}(\beta \mathbf{g}(T - T_0)). \tag{6}$$

In this case, boundary conditions for pressure are a direct consequence of the boundary conditions for the velocity **u** and its addition **w** set in the problem. For example, in the case of an impermeable solid wall, the boundary conditions can be specified as zero velocity components normal to the boundary, $\mathbf{u}_n = 0$, and the zero addition $\mathbf{w}_n = 0$. These two conditions straightforwardly imply a boundary condition for pressure of the form

$$\nabla p = -\rho_0 \beta \mathbf{g}(T - T_0). \tag{7}$$

To perform computations based on the QHD system, it is necessary to choose a suitable regularization parameter τ. If τ is too large, the terms proportional to τ (regularizers) begin to dominate, which leads to a distortion of the numerical solution and then to its destruction. If τ is too small, then an unacceptably small time step is required for the stability of the numerical solution. Numerical experience suggests that, starting from a certain value, a decrease in τ ceases to affect the accuracy of the numerical solution. The choice of the regularization parameter determines the stability, accuracy, and labor intensity of the algorithm, so its optimal value should be chosen in computations.

Computational practice suggests that the integration time step Δt ensuring the conditional stability of the difference algorithm is close to τ.

The order of the base value of the coefficient τ_0 is determined by the condition that the coefficient in front of the viscous terms exceeds the value of the regularization parameter. For this purpose, we nondimensionalize the momentum equation (2) and estimate the values of the coefficients on its right-hand side. The coordinates, time, velocity, pressure, and temperature are normalized by H, $\frac{H}{u_0}$, u_0, $\rho_0 u_0^2$, ΔT, respectively, where H and u_0 are the characteristic length and speed in the problem and ΔT is the temperature difference between the walls. After passing to dimensionless variables, Eq. (2) retains its form, but dimensionless coefficients appear in the terms on its right-hand side, namely, the coefficient $\frac{\nu}{Hu_0} = \frac{1}{\mathrm{Re}}$ before the viscous terms, $\frac{\tau u_0}{H}$ before the additional terms, and $\frac{\beta g \Delta T H}{u_0^2}$ before the buoyancy term. Comparing the coefficients multiplying the first and second terms on the right-hand side of equation, we obtain the following condition on the value of τ_0:

$$\tau = \tau_0 = \frac{\nu}{u_0^2} = \frac{\nu}{\beta g \Delta T H}. \tag{8}$$

Here, the characteristic flow speed is chosen in the form $u_0^2 = \beta g \Delta T H$, which is accepted in natural convection problems. Then the dimensionless coefficient in the buoyancy term becomes equal to 1. With the chosen nondimensionalization procedure, the dimensionless parameter τ_{0nd} is related to the Grashof number $\mathrm{Gr} = \frac{\beta g \Delta T H^3}{\nu^2}$ as follows: $\tau_{0nd} = \frac{1}{\sqrt{\mathrm{Gr}}}$. For computations, the parameter τ should be chosen in the form $\tau \le \tau_0$.

A spatial approximation is constructed using the finite volume method with all spatial derivatives calculated using central differences. An explicit time difference scheme is used, while the terms with molecular viscosity are approximated implicitly. The stability of the algorithm is ensured by artificial dissipation, whose value is adjusted by its nonlinear structure depending on the gradients of pressure, temperature, and velocity.

2. THERMAL CONVECTION PROBLEM IN A SQUARE CAVITY

Due to the simplicity of its formulation and the clarity of results, thermal convection in a square cavity has long been a convenient benchmark problem for demonstrating the properties of numerical algorithms (see, e.g., recent works [4, 5, 8]). At low Grashof numbers, the flow is steady; for $\mathrm{Gr} \ge 2 \times 10^8$, undamped oscillations are established in the region, which can subsequently be transformed into a two-dimensional analogue of turbulent flow.

In [11–14] the QHD algorithm was tested on this problem at low Grashof numbers corresponding to steady flow, namely, at $\mathrm{Gr} = 10^3, 10^4, 10^5$. The numerical results were compared with data produced by a second-order accurate method constructed in the stream function–vorticity variables and with experi-

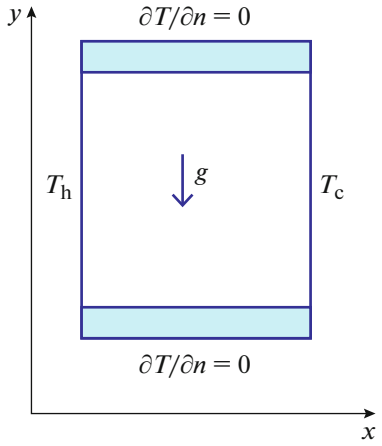

Fig. 1. Computational domain. A hot wall at the temperature T_h, is on the left, while a cold wall at the temperature T_c is on the right.

mental data. It was shown that the QHD algorithm remains highly accurate even on coarse grids. Additionally, the convergence of the solution under mesh refinement and the influence of τ on the solution were demonstrated. Specifically, it was shown that the optimal value of the regularization parameter is given by (8). The accuracy of the solution is not improved with decreasing τ and degrades with increasing τ. Below, we discuss numerical solutions of this problem obtained using OpenFOAM at high Grashof numbers.

A schematic view of the computational domain and the setting of boundary conditions for temperature are shown in Fig. 1.

The computational domain is a square with side length H. The system is in the gravity field $g = 9.81$ m/s^2. The upper and lower walls are adiabatic, the left wall is hot, and the right wall is cold. On the boundaries of the domain, we set no-slip and impermeability conditions for velocity. The boundary conditions for pressure are given by (7). This means that the normal derivative of pressure on the vertical walls is set to zero, while the normal derivative of pressure on the horizontal walls is determined by the temperature. In other words, the condition $\dfrac{\partial p}{\partial \mathbf{n}} = -\beta\rho_0\mathbf{g}(T - T_0)$ is set on the upper and lower walls, and the condition $\dfrac{\partial p}{\partial \mathbf{n}} = 0$ is specified on the side walls. For velocity, the no-slip condition $\mathbf{U} = 0$ is set at all the boundaries. The upper and lower walls are assumed to be heat-insulated: $\dfrac{\partial T}{\partial \mathbf{n}} = 0$.

The numerical simulation of the viscous incompressible flow was performed using the mulesQHDFoam solver implemented in OpenFOAM. All quantities are dimensional and given in SI units. Numerical results are also presented in SI units, except for the data in Table 3, which are given in dimensionless form for comparison with reference data.

The two-dimensional computations were carried out using the three-dimensional algorithm with the third dimension represented by a single cell. All computations were performed on uniform spatial grids with square cells.

Initially, the fluid was at rest, the pressure was equal to its atmospheric value, the temperature in the domain was $T = T_0 = 293.15$ K (20°C), the temperature of the left wall was $T_h = 313.15$ K, and the temperature of the right wall was $T_c = 273.15$ K.

As a working fluid, we used air. The air parameters required for the computations are given Table 1.

The Grashof number was computed using the formula $\mathrm{Gr} = \dfrac{\beta g \Delta T H^3}{\nu^2}$ with $\Delta T = 40°$. The Prandtl number in the computations was set to unity, so the Rayleigh number was $\mathrm{Ra} = \mathrm{Pr} \cdot \mathrm{Gr} = \mathrm{Gr}$. The results of [4] show that, for air, the difference between $\mathrm{Pr} = 0.7$ and $\mathrm{Pr} = 1$ has a very small effect on the values of the velocities in this problem.

Table 1. Dimensional parameters of air at normal pressure and temperature of 20°C

Dynamic viscosity μ	18.1×10^{-6} kg/(m s)
Kinematic viscosity ν	15.06×10^{-6} m^2/s
Thermal expansion coefficient β	3.43×10^{-3} K^{-1}
Density ρ_0	1.205 kg/m^3
Heat capacity at constant pressure C_p	1005 J/(kg K)

Table 2. Size of the computational domain for various Grashof numbers

No	Gr	H, cm	τ, s
1	10^4	1.190	9.4×10^{-4}
2	10^5	2.565	4.3×10^{-4}
3	10^6	5.530	2.0×10^{-4}
4	10^7	11.900	9.4×10^{-5}
5	10^8	25.650	4.3×10^{-5}
6	2×10^8	32.300	3.5×10^{-5}
7	10^9	55.300	2.0×10^{-5}

The number Gr was changed by varying the size of the domain. Consistent values of the Grashof number, the parameter τ, and the size of the domain are given in Table 2.

The following reduced values of τ were used in the computations: $\tau = 10^{-4}$ for $\mathrm{Gr} = 10^4, 10^5, 10^6$ and $\tau = 10^{-5}$ for $\mathrm{Gr} = 10^7, 10^8, 10^9$. The time step was 2×10^{-4} for $\mathrm{Gr} = 10^4, 10^5, 10^6, 10^7, 10^8$ and 2×10^{-5} for $\mathrm{Gr} = 2\times10^8, 10^9$. As initial conditions in variants 1–3, we used zero velocities and the temperature in the domain specified as $T = T_0 = 20$°C. In variants 4 and 5, we used both the same initial conditions and the numerical results obtained for the problem with a lower value of Gr on the corresponding grid. Steady flow regimes are independent of the initial conditions used.

Figures 2–6 show the steady-state velocity and temperature fields obtained in the thermal convection problem on a 40 × 40 grid for the Grashof numbers given in Table 2. Streamlines (left) and isotherms (right) are shown for $\mathrm{Gr} = 10^4, 10^5$ at $t = 40$ s and for $\mathrm{Gr} = 10^6, 10^7, 10^8$ at $t = 100$ s.

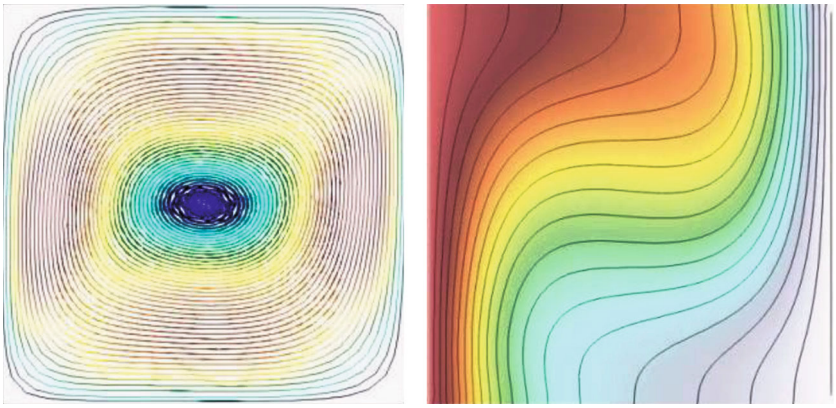

Fig. 2. $\mathrm{Gr} = 10^4$.

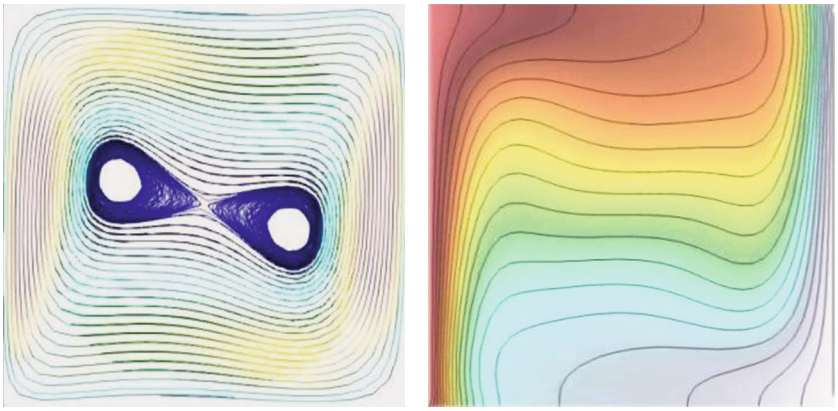

Fig. 3. $\mathrm{Gr} = 10^5$.

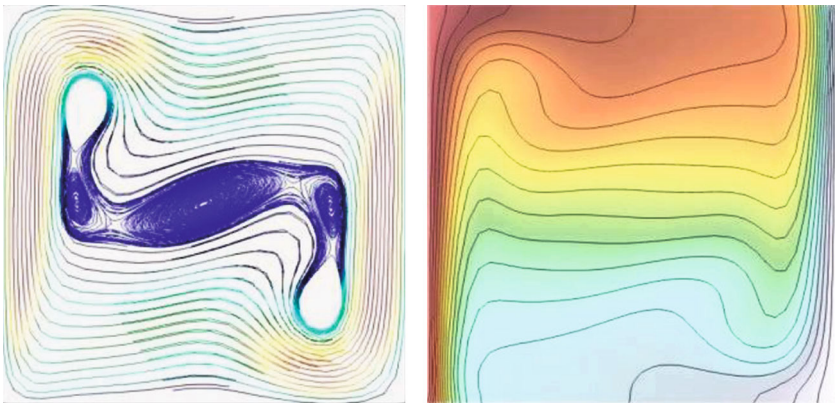

Fig. 4. $\mathrm{Gr} = 10^6$.

Figures 2–6 confirm the evolution of the flow with increasing Gr known from a number of publications. Specifically, at $\mathrm{Gr} = 10^4$, the flow is a vortex close to a circle, which distorts the temperature field. As the Grashof number increases, the shape of the vortex flow also begins to distort. At $\mathrm{Gr} = 10^8$ the vortex strongly stretches in the horizontal direction and contracts in the vertical. Away from the walls, the horizontal temperature gradient nearly vanishes, while the gradient near the vertical walls increases significantly. In the flow core, the temperature actually varies only in the vertical.

For velocity components, Fig. 7 presents a typical pattern of reaching a steady state for $\mathrm{Gr} = 10^8$ at points 1 and 2 with coordinates (0.064, 0.064, 0.0) and (0.064, 0.192, 0.0).

For quantitative evaluation of the numerical results, they were compared with those of [4, 5], where thermal convection in a square cavity was computed in the stream function–vorticity variables on fine grids. In [4] a high-order accurate algorithm with a quasi-wavelet-based discrete singular convolution (DSC) was compared with the Galerkin finite-element method. A third-order upwind scheme (Opt-UCD3) in the stream function–vorticity variables was used in [5]. It was shown in [4] that the flow is steady for $\mathrm{Gr} \le 10^8$, and an unsteady oscillation flow regime is formed at $\mathrm{Gr} = 2\times10^8$.

In Table 3, our results for flow velocity are compared with the data [4, 5] and the results of the studies referenced therein. The comparison is carried out for the maximum horizontal velocity nondimensionalized according to [4, 5]: $\tilde{u}_x = u_{x\,\mathrm{dim}}\dfrac{H}{\nu}$, $t = \tilde{t}\dfrac{H^2}{\nu}$. Dimensionless variables are denoted by a tilde.

Additionally, Table 3 presents the values of the maximum dimensionless velocity $\tilde{u}_x$ in the y coordinate at $x = 0.5H$.

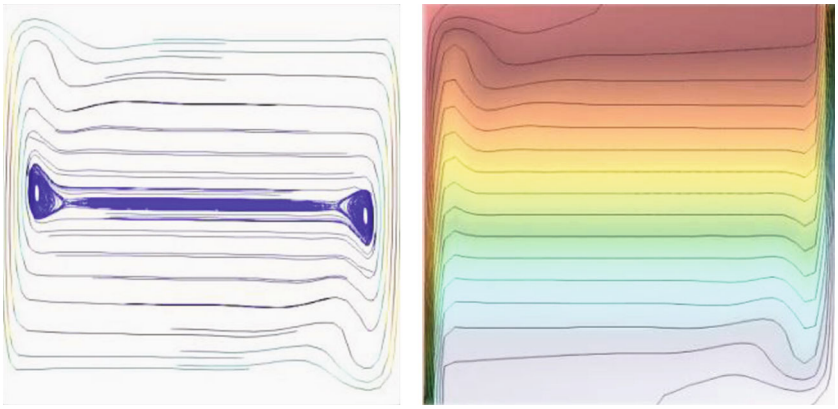

Fig. 5. $\mathrm{Gr} = 10^7$.

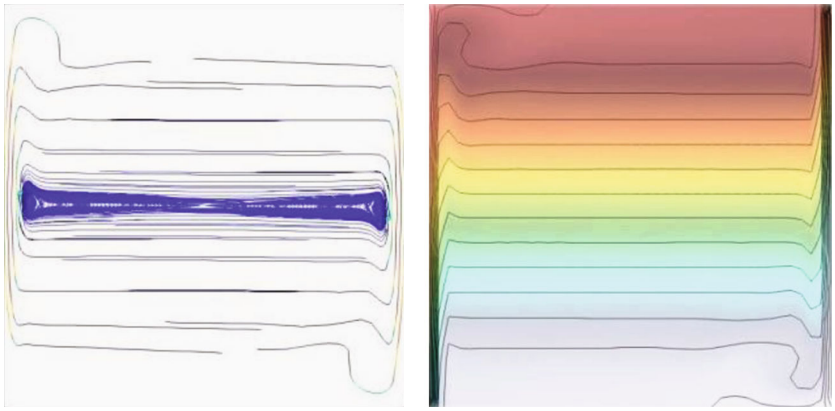

Fig. 6. $\mathrm{Gr} = 10^8$.

Inspection of Table 3 shows that the QHD results obtained on a 40 × 40 grid at $\mathrm{Gr} = 10^4$, 10^5 agree well with the data of [4], obtained on a 101 × 101 grid. For $\mathrm{Gr} = 10^6$ the QHD algorithm requires an

Table 3. Summary of present computations and their comparison with the results of [4, 5]

Grashof number Gr	Maximum dimensionless horizontal speed $\tilde{u}_x$, present computation	Maximum dimensionless horizontal speed $\tilde{u}_x$ [4], speed range for methods from [4]
10^4	16.02, 40 × 40 grid	15.967, 15.967–16.2
10^5	33.30, 40 × 40 grid	33.51, 33.39–34.81
10^6	52.36, 40 × 40 grid 65.40, 80 × 80 grid 65.43, 160 × 160 grid	65.55, 64.6912–65.55
10^7	125.11, 40 × 40 grid	145.06, 139.7–145.266
10^8	250.00, 40 × 40 grid 281.50, 80 × 80 grid 296.52, 160 × 160 grid	295.67, 283.689–296.71
2×10^8	282.46, 40 × 40 grid 342.95, 80 × 80 grid Oscillations, 160 × 160 grid Oscillations, 320 × 320 grid	Oscillations [5]

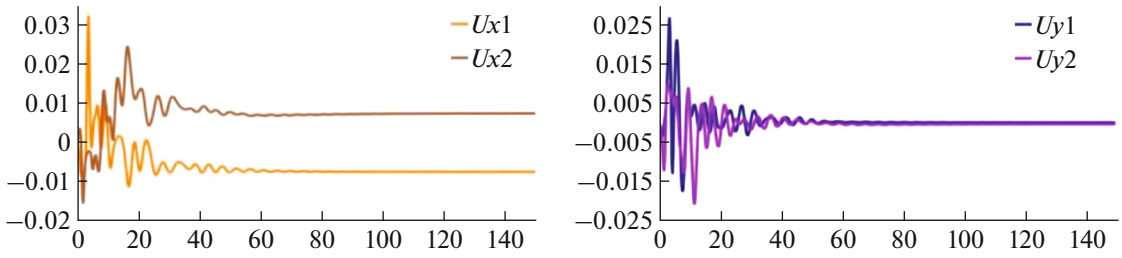

Fig. 7. Distributions of velocity components at points 1 and 2 for $\mathrm{Gr} = 10^8$, 40 × 40 grid.

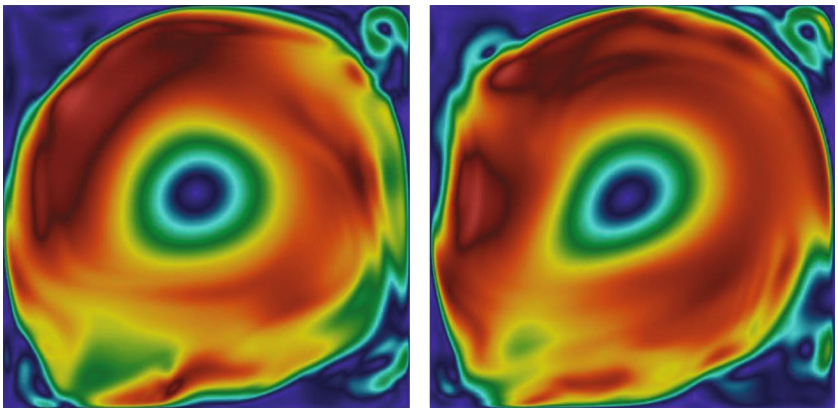

Fig. 8. Velocity magnitude. Maximum values are 0.53 and 0.51 m/s.

80 × 80 grid to agree with the results of [4] obtained on a 101 × 101 grid. For this variant, the QHD results exhibit convergence under mesh refinement. At $\mathrm{Gr} = 10^7$ a finer spatial grid is required for achieving the prescribed accuracy. A 301 × 301 grid was used in [4]. At $\mathrm{Gr} = 10^8$, the accuracy achieved on a 160 × 160 grid corresponds to the 301 × 301 grid in [4].

In [5] this problem was computed on a 129 × 129 grid at $\mathrm{Gr} = 10^4, 10^5, 10^6$ and a 257 × 257 grid at $\mathrm{Gr} = 10^8$. For steady regimes, the results of [4, 5] are close to each other.

The onset of unsteady flow regimes in a square cavity for the Grashof numbers $\mathrm{Gr} = 2\times10^8$ and $\mathrm{Gr} = 10^9$ was obtained and analyzed in [5]. These regimes were also produced by the QHD algorithm in the case of mesh refinement.

At $\mathrm{Gr} = 2\times10^8$, a steady flow is formed on 40 × 40 and 80 × 80 grids. On a 160 × 160 grid, the QHD algorithm yields an undamped nonperiodic solution, which agrees with the one obtained on a 257 × 257 grid in [5]. As an initial condition, we used the flow field obtained at $\mathrm{Gr} = 10^6$. Figures 8 and 9 display typical velocity and temperature fields at various times obtained for this case.

Figure 10 presents the velocity components and temperature vs. time at points 1 and 2 with respective coordinates (0.08, 0.08, 0.0) and (0.08, 0.242, 0.0) for $\mathrm{Gr} = 2\times10^8$. The results were obtained on a 320 × 320 grid. As an initial condition, we also used the steady-state solution obtained at $\mathrm{Gr} = 10^6$.

3. THERMAL CONVECTION IN H:8H RECTANGULAR CAVITY

In a cavity that is an elongated rectangle, oscillation regimes develop at lower Grashof numbers. Experimental and numerical studies of such flows are presented in [2, 6–9]. In an experiment with ethyl alcohol [2] (Pr ~ 20) the most intense chaotic oscillations were observed near the upper and lower boundaries of the cavity, while a stagnant zone with weaker oscillations was formed in the center of the region.

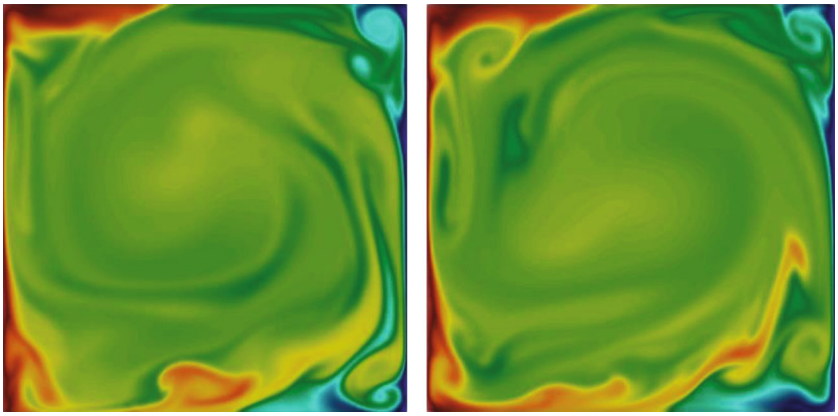

Fig. 9. Temperature. Range of variation is from 270 to 310 K.

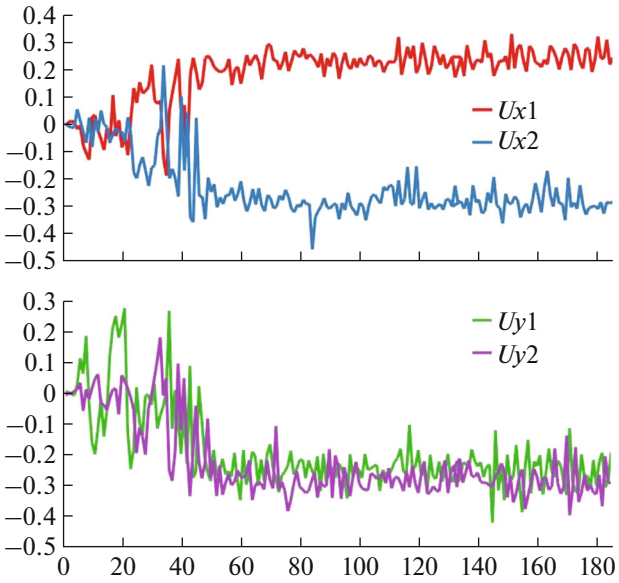

Fig. 10. Velocity components at points 1 and 2 as functions of time for $\mathrm{Gr} = 2\times10^8$, 320 × 320 grid.

The formulation of the problem presented below corresponds to a classical numerical test described in detail in [6–8], where variants of undamped chaotic flow oscillations in a cavity with the width-to-height ratio H:8H were studied at the Rayleigh number $\mathrm{Ra} = 3.4\times10^5$.

In the computation described below, we used a domain of the same configuration with flow parameters $\mathrm{Pr} = 1.0$ and $\mathrm{Ra} = \mathrm{Gr} = 3.4\times10^5$. In dimensional form, the side lengths of the rectangle were 0.03855 and 0.3084 m, respectively. Estimate (8) for the dimensional regularization parameter was found to be $\tau = \dfrac{\nu}{\beta g \Delta T H} = 3\times10^{-4}$. The time step was 10^{-4}. We used 48 × 240 and 96 × 240 grids.

For the regularization parameter $\tau = 3\times10^{-4}$, a steady-state distribution of flow parameters was obtained in the computation. A decrease in τ to the value $\tau = 5\times10^{-5}$ allowed us to simulate an unsteady, nearly chaotic flow in the domain. The initial value for the computation was the steady regime obtained at $\tau = 3\times10^{-4}$. Figure 11 presents contour lines for the velocities u_x, u_y, temperature T, and particle trajectories for the solution computed on a 96 × 240 grid and averaged over the time interval 250–270. In the case of the averaging interval 120–250, the averaged results remain nearly unchanged.

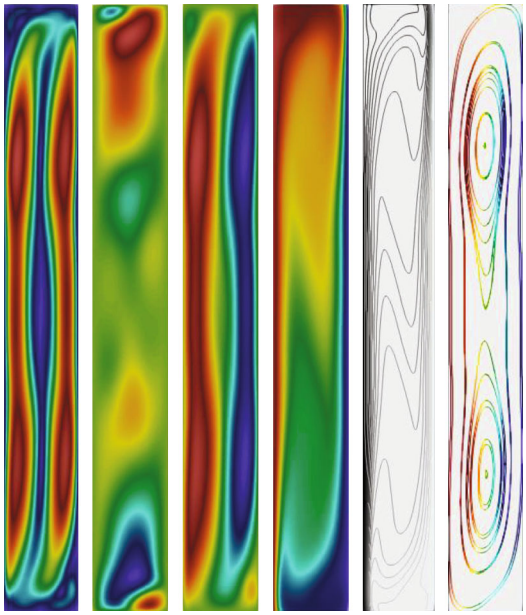

Fig. 11. Averaged flow field: velocity magnitude, u_x, u_y, T, isotherms, and streamlines.

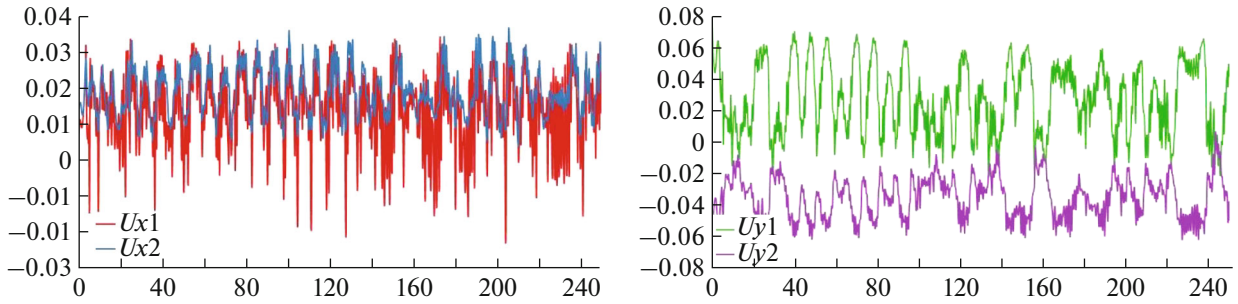

Fig. 12. Velocity components at points 1 and 2 as functions of time.

Figure 12 shows the evolution of the velocity components over time at point 1 (0.007 0.284 0.0), i.e., near the upper left corner of the cavity, and at point 2 (0.03 0.29 0.0), i.e., near the upper right corner of the cavity until the time $t = 270$.

In [6] the unsteady flow for this problem was numerically simulated on much finer grids with a minimum number of 75 × 600 nodes. In [7, 8] the unsteady flow for this problem obtained on 252 × 252 and 96 × 480 grids, respectively, was nearly regular. The averaged flow field shown in Fig. 11 qualitatively agrees with the fields presented in [6, 8, 9]. The best agreement between the isotherms in [6, 8, 9] and the QHD results is observed in the center and near the boundaries of the rectangular domain. The evolution curves in Fig. 12 qualitatively agree with [9], where the computations were carried out on a 100 × 800 grid.

4. CONCLUDING REMARKS

The numerical experiments have shown that the QHD algorithm as applied to thermal convection problems is able to simulate both steady flows and the formation of unsteady regimes observed with increasing Grashof number. To model these problems adequately, it is necessary to choose an appropriate mesh size to resolve boundary layers and to select a regularization parameter determining smoothing in the algorithm.

A comparison of the obtained numerical solutions with reference results for flows in square and rectangular cavities showed that the QHD algorithm is not inferior in accuracy to the reference methods. Moreover, the required accuracy of velocity computation is achieved on coarser grids than in algorithms

of more complex structure with a higher order of approximation. The QHD algorithm also yields the onset of oscillation regimes at Grashof numbers known from benchmark computations.

Thus, the QHD algorithm implemented in the OpenFOAM package seems promising for solving thermal convection problems.

FUNDING

This work was supported by ongoing institutional funding. No additional grants to carry out or direct this particular research were obtained.

CONFLICT OF INTEREST

The authors of this work declare that they have no conflicts of interest.

REFERENCES

1. G. Z. Gershuni, E. M. Zhukhovitskii, and A. A. Nepomnyashchii, *Stability of Convective Flows* (Fizmatlit, Moscow, 1989) [in Russian].
2. B. S. Berdnikov and V. A. Grishkov, "Laminar–turbulent transition in a free convective boundary layer and heat transfer in vertical walls," *Proceedings of the 4th Russian National Conference on Heat Transfer*, Vol. 3: *Free Convection and Heat and Mass Transfer in Chemical Transformations* (2006). pp. 67–70.
3. A. I. Prostomolotov and N. A. Verezub, *Mechanics of Producing Crystalline Materials* (Nats. Issled. Tech. Univ. "MISiS," Moscow, 2023) [in Russian].
4. D. C. Wan, B. S. Patnaik, and G. W. Wei, "A new benchmark quality solution for the buoyancy-driven cavity by discrete singular convolution," Numer. Heat Transfer Part B **40**, 199–228 (2001).
5. B. Zhao and Z. Tian, "High-resolution high-order upwind compact scheme-based numerical computation of the natural convection flows in a square cavity," Int. J. Heat Mass Transfer **98**, 313–328 (2016).
6. B. Trouette, "Lattice Boltzmann simulations of a time-dependent natural convection problem," Comput. Math. Appl. **66** (8), 1360–1371 (2013).
7. J. Oder and I. Tisely, "Spectral benchmark for natural convection flow in a tall differentially heated cavity," *22nd International Conference Nuclear Energy for New Europe September 9–12, 2013, Bled-Slovenia*.
8. N. B. Cheikh, B. B. Beya, and T. Lili, "Benchmark solution for time-dependent natural convection flows with an accelerated full-multigrid method," Numer. Heat Transfer, Part B: Fundam. **52** (2), 131–151 (2007). https://doi.org/10.1080/10407790701347647
9. Y.-L. Feng, S.-L. Guo, W.-Q. Tao, and P. Sagaut, "Regularized thermal lattice Boltzmann method for natural convection with large temperature differences," Int. J. Heat Mass Transfer **125**, 1379–1391 (2018). https://doi.org/10.1016/j.ijheatmasstransfer.2018.05.051.hal-02114047
10. S. V. Polyakov and A. G. Churbanov, Preprint No. 145, IPM RAN (Keldysh Inst. of Applied Mathematics, Russian Academy of Sciences, Moscow, 2019).
11. Yu. V. Sheretov, *Continuum Dynamics under Spatiotemporal Averaging* (Regulyarnaya i Khaoticheskaya Dinamika, Moscow–Izhevsk, 2009) [in Russian].
12. T. G. Elizarova, *Quasi-Gas Dynamic Equations* (Nauchnyi Mir, Moscow, 2007; Springer, Berlin, 2009).
13. T. G. Elizarova and Yu. V. Sheretov, "Theoretical and numerical analysis of quasi-gasdynamic and quasi-fluid-dynamic equations," Comput. Math. Math. Phys. **41** (2), 219–234 (2001).
14. T. G. Elizarova, I. S. Kalachinskaya, A. V. Klyuchnikova, and Yu. V. Sheretov, "Application of quasi-hydrodynamic equations in the modeling of low-Prandtl thermal convection," Comput. Math. Math. Phys. **38** (10), 1662–1671 (1998).
15. M. V. Kraposhin, D. A. Ryazanov, and T. G. Elizarova, "Numerical algorithm based on regularized equations for incompressible flow modeling and its implementation in OpenFOAM," Comput. Phys. Commun. **271**, 108216 (2022).
16. M. A. Kiryushina, T. G. Elizarova, and A. S. Epikhin, "Numerical modeling of a melt flow by the Czochralski method in the OpenFOAM package using a quasi-hydrodynamic algorithm," Math. Models Comput. Simul. **15** (Suppl. 1), S131–S142 (2023).

Translated by I. Ruzanova